Magnetic Mesoporous Nanocarriers for Drug Delivery with Improved Therapeutic Efficacy

*Albert Serrà, Núria Gimeno, Elvira Gómez, Margarita Mora, Maria Lluïsa Sagristá, and Elisa Vallés**

Mesoporous CoNi@Au core@shell nanorods are synthesized as magnetic drug nanocarriers by electrodeposition using ionic liquid-in-aqueous microemulsions. Mesoporous nanorods present a highly effective area (186 $m^2 g^{-1}$) and magnetic character that allows their manipulation, concentration, and retention by applying a magnetic field. The nanorods have been functionalized with thiol-poly(ethyleneglycol) molecules, and molecules of Irinotecan, a drug used in chemotherapy, are retained in both the lattice of the linked thiol-poly(ethyleneglycol) molecules and inside the interconnected nanorods pores. The nanorods' mesoporous character allows a high drug-loading capability and magnetic behavior that allows the drug's controlled release. A high cellular viability of HeLa cells is obtained after their incubation with the nanorods functionalized with thiol-poly(ethyleneglycol). However, when the nanorods function as carriers for Irinotecan, significant cell death is occurred when HeLa cells are incubated with the functionalized, drug-loaded nanorods. Cell death is also produced by applying an alternating magnetic field due to both the effect of the release of Irinotecan from the carrier as to mechanical damage of cells by nanorods subjected to the effect of a magnetic field. The proposal to used mesoporous magnetic nanorods as drug carriers can thus dramatically reduce the amounts of both nanocarrier and drug needed to efficiently destroy cancer cells.

1. Introduction

Different types of nanomaterials – polymeric micelles, dendrimers, liposomes, nanoparticles, and nanorods, among others – have been proposed as drug delivery systems and, in recent decades, have been studied extensively as powerful tools to improve therapeutic efficacy.[1] More recently, intensive research has sought to design novel smart nanocarriers of drugs to control therapeutic outcomes, target modalities toward specific diseases, and minimized side effects.[2] The effect of the drug delivery system on the activity, localization, and tumor accumulation of different drugs has been investigated. Thus, we have already procured liposomes, micelles, and other solubilizing products to carry photosensitizers for photodynamic therapy and camptothecins for chemotherapy, and their usefulness has been assessed by using healthy and cancerous cell lines, for in vitro experiments, and DBA/2 tumor bearing mice, for in vivo assays.[3] By extension, researchers have also explored using environmentally responsive smart nanocarriers that can improve pharmacological efficacy due to physicochemical changes that occur during exposure to external stimuli. These stimuli, which can be combined to further enhance pharmacologic activity, include light, temperature, ultrasound, magnetic field, electrical field, and chemical signals such as pH, ionic strength, redox potential, and enzymatic activities.[4] Using nanocarriers combined with external or internal stimuli improves the control of drug delivery over that of traditional release systems in vivo (i.e., passive delivery programed prior to implantation) that cannot be modified during the needs of therapeutic change. As such, nanomaterials have the potential to revolutionize the diagnostic and therapy of cancer, one of the world's most devastating diseases. They could be of particular use with colorectal cancer, the third most common cause of cancer deaths among both men and women in the United States and Europe, as well as the second most common lethal cancer overall.[5]

Current cancer treatments involve surgical intervention, radiation, and chemotherapy, typically accompanied by toxic side effects that limit the drug dosage that can be given to a patient, since not all the tumor tissues can be exposed to a lethal dose of the drug.[6] In the last decade, several new cytotoxic agents have been explored for colorectal cancer treatment. Among them, irinotecan (CPT-11), a water-soluble semisynthetic camptothecin derivative of the Topoisomerase I family of interactive compounds, is used in current chemotherapy protocols for a range

A. Serrà, N. Gimeno, Dr. E. Gómez, Dr. E. Vallés
Grup d'Electrodeposició de Capes Primes i Nanoestructures (GE-CPN)
Departament de Ciència de Materials i Química Física, and Institut de Nanociència i Nanotecnologia (IN2UB)
Universitat de Barcelona
Martí i Franquès 1, E-08028 Barcelona, Catalonia, Spain
E-mail: e.valles@ub.edu
Dr. M. Mora, Dr. M. L. Sagristá
Grup d'Aplicacions Biomèdiques de Sistemes Col·loidals
Departament de Bioquímica i Biomedicina Molecular
Facultat de Biologia
Universitat de Barcelona
Avinguda Diagonal 643, E-08028 Barcelona, Catalonia, Spain

DOI: 10.1002/adfm.201601473

of tumor diseases.[7] Such findings are important because using nanostructured materials as carriers can significantly improve the pharmacological properties of drugs, by encouraging the drug's accumulation in the target tissue. Their unique properties can also enhance therapeutic efficacy with the application of specific external stimuli, which as triggers in drug delivery systems enable a spatially, temporally, or even spatiotemporally controlled release that can play a major role in sustained release systems.[8]

At the same time, designing carriers capable of selectively releasing their payloads at target sites in the body has special relevance in drug delivery systems. Special attention was given to receptor mediated delivery systems, in particular, those targeted to folate receptor that has been shown to increase the uptake of the entrapped drugs by folate receptor positive cells.[9] In that context, magnetic nanocarriers represent a promising opportunity because they can be concentrated and kept with an external field.[10] In recent years, increased efforts have been put toward developing magnetic nanomaterials for nanobiomagnetic applications, including the use of magnetic resonance imaging contrast agents, targeted drug delivery, bioseparation, and magnetically induced hyperthermia.[10,11] Those applications are possible because magnetic nanomaterials, especially magnetic nanoparticles, can be remotely manipulated by magnetic fields. Crucial to such biological applications is a quasi-zero magnetization remanent state, which prevents the magnetic agglomeration of nanomaterials by virtue of their interaction with remanent moments, which in turn stabilizes the nanomaterial's suspension.[12] By extension, surface functionalization could be used to minimize their aggregation.[13] Via hyperthermia or mechanical destruction of cells, magnetic nanomaterials can furthermore be heated or rotated, respectively, under alternating fields during cancer therapy.[14] Altogether, the integration of magnetic materials with biological molecules into chemotherapy can generate smart hybrid materials with promising advanced properties.

Herein, we propose the synthesis of magnetic mesoporous CoNi@Au core@shell nanorods, 100 nm in diameter and ≈2 µm long, by electrodeposition using ionic liquid-in-aqueous solution (IL/W) microemulsions to be used as delivery systems for therapeutic molecules. The objective of this study was to obtain smart drug nanocarriers that met four criteria: First, nanorod shape and high density of interconnected mesopores needed to offer a surface area conducive to supporting high quantities of drugs. Second, magnetic actuation needed to radically enhance therapeutic efficacy by allowing easy manipulation, magnetic targeting, mechanical destruction, and better control of drug release through high saturation magnetization (M_s) and low remanence (M_r). Third, low cytotoxic effects and high biocompatibility were needed to achieve high cellular viability in the presence of carriers. Fourth, the nanocarriers needed to demonstrate ease of functionalization, retention, and release of drugs. To test the applicability of nanocarriers, the CPT-11 drug was analyzed for its retention and posterior release from the nanocarrier, in magnetic stirring and non-stirring conditions. The high surface area and the high drug-loading capability of the CoNi@Au mesoporous nanorods, the controlled release of the drug by means of a magnetic field, the uptake of the nanorods in the interior of the test HeLa cells, and the cellular death of the test cells by both the release of the carcinogenic drug and the mechanical destruction of the cells by the rotating magnetic field applied make the new nanostructures excellent candidates for increased therapeutic efficiency. In sum, the findings of our study could contribute to reducing the amount of drug nanocarriers in a therapeutical treatment and thus bringing about more efficient carcinogenic cell destruction.

2. Results and Discussion

This paper presents the possibility of using magnetic compact or mesoporous nanorods as nanocarriers for drugs. In biomedical applications, nanorods offer advantages over other magnetic nanostructures, including higher magnetic moments per unit of volume and larger surface-to-volume ratios, especially in the case of mesoporous rods. Although Fe and Ni nanorods have been proposed for some biomedical applications,[15] we propose using CoNi@Au nanorods, largely because they present high M_s and improved chemical stability.[13b,16] In doing so, we acknowledge the well-known fact that the toxicity of such materials, dependent on their contents in biological media, is extremely low and can be eliminated from the body in a relatively short time.[10] Moreover, the formation of a gold shell over the entire surface of the nanorods prevents the dissolution of the metals, while the functionalization of core@shell nanorods with long poly(ethyleneglycol) (PEG) molecules makes them hydrophilic and minimizes their aggregation. Ultimately, we propose the synthesis of new nanorods as drug carriers for pharmacologic treatments in cancer therapy. Along with the functionalization of drug-loaded nanorods, using these devices would make it possible to deliver specific drugs to tumor tissues by way of a magnetic field, which would dramatically increase the benefits of treatment.

2.1. Nanocarriers Fabrication and Characterization

Electrodeposition in potentiostatic conditions was used as a synthetic route for preparing mesoporous and compact nanorods, using microemulsions with ionic liquids and aqueous solutions as electrochemical media, respectively.[17] After synthesis and washing, the magnetic nanorods were immersed in a gold salt solution to form a gold shell by galvanic displacement under ultrasound stirring. Synthesis is illustrated in **Figure 1**. We combined the use of a soft template (i.e., microemulsion) for pore definition and a hard template (i.e., polycarbonate membranes) for nanorods growth in order to control of the length, diameter, and pore size by way of controlling the deposition time, hard template type, and the microemulsion structure, respectively. Notably, this method affords mesoporous or compact nanorods of numerous metallic and compositions, all by controlling the composition of the aqueous solution and selecting the deposition potential.

Earlier, to electrodeposit nanorods inside the polycarbonate membranes, we analyzed the electrodeposition process in the three electrochemical media: microemulsion (i.e., to obtain mesoporous nanorods), aqueous solution (i.e., to obtain compact

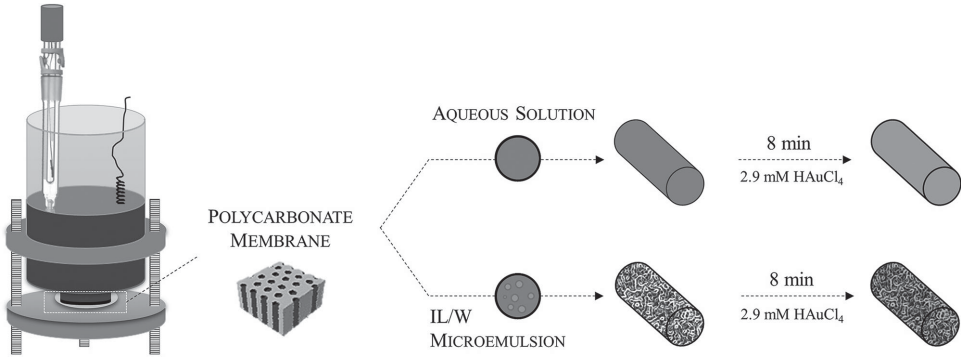

Figure 1. Schematic representation of electrochemical synthesis of magnetic CoNi@Au NRs in aqueous solution and IL/W microemulsions.

nanorods), and an aqueous-surfactant mixture (i.e., to understand the surfactant effect). It is possible to electrodeposit CoNi from the three types of electrochemical media (Supporting Information) inside the nanochannels of polycarbonate (PC) membranes, which also allows the selection of the most adequate deposition potential in order to ensure the desired composition and deposition rate. The voltammetric study (see Supporting Information) of the CoNi system reveals a different voltammetric profile in presence of either the microemulsion or aqueous-surfactant mixture in respect to the classical profile in the aqueous solution. The first reduction peak occurred at around –0.6 V, assigned to the initial nickel deposition, followed by a primary reduction from –0.8 V, assigned to the simultaneous codeposition of nickel and cobalt and a single oxidation peak, corresponding to the alloy oxidation in the anodic scan. However, with microemulsion, a lower j/E slope occurred due to the lower deposition rate in the more viscous microemulsion medium than in the aqueous solution. A similar Q_{ox}/Q_{red} ratio in the voltammetric process reflects the dismal participation of hydrogen evolution in both media.

The viscosity, surface tension, and conductivity (Table 2S, Supporting Information) of the three electrodeposition media were also measured to corroborate the possibility of filling the nanochannels of the PC membrane. From the voltammetric study, a deposition potential of –1000 mV for the different electrochemical media with a relatively high deposition rate was selected, thereby ensuring comparable homogeneous growth comparable in three different systems in terms of efficiencies and alloy composition (Table 1S, Supporting Information).

Chronoamperometric curves of synthesis (Figure 2Sa, Supporting Information) in stationary conditions evolved to quasi stationary values, which reflect a constant growth regime. The deposition rate was greater with compact nanorods (i.e., aqueous solution) due to the lower viscosity of the medium. Nanorods were released from the PC membrane and, after thorough washing, immersed in a gold solution, which resulting in the formation of a thin gold shell due to galvanic displacement. As scanning electron microscopy showed (Figure 2Sb,c, Supporting Information) nanorods maintained their integrity after the formation of the Au shell, and nanorods of similar lengths (Figure 2Sc, Supporting Information) and diameter emerged in both electrochemical media. Both types of nanorods exhibit similar composition before Au shell formation, which demonstrates that using electrodeposition with selected baths and conditions allows the preparation of CoNi nanorods with modulated composition. However, as **Table 1** depicts, mesoporous nanorods contained a significantly more Au after the galvanic displacement, as could be expected due to their significantly greater area.

We characterized the morphology of the prepared nanorods by way of transmission electron microscopy (**Figure 2**), representative images of which reveal significant differences according to preparation approach. Nanorods obtained in aqueous solution displayed compact morphology and a diameter of 104 ± 9 nm, dispersion likely due to the insufficient uniformity of nanochannels in the PC membrane (Figure 2a). By contrast, IL/W microemulsions yielded mesoporous nanorods with a high density of well-defined nonspherical mesopores over the entire area, even at the inner part of the wires that formed an ordered, interconnected pore network with easy accessibility (Figure 2b). The diameter of the mesoporous nanorods was of 107 ± 12 and the size of the mesopores of ≈2–4 nm. The average size of mesopores was coherent since ionic liquid droplets (hydrodynamic diameter = 12.4 nm; polydispersity index = 0.08) were slightly larger. This result is unsurprising because pores are defined by the size of ionic liquid droplets, which should be smaller than the hydrodynamic diameter determined by dynamic light scattering (DLS).

Table 1. Working potential, deposition charge, length, diameter, elemental composition, and shell thickness of nanorods.

	Potential [mV]	Deposition charge [C]	Length [μm]	Diameter [nm]	Elemental composition [wt%]			Shell thickness [nm]
					Co	Ni	Au	
Compact CoNi@Au	–1000	–2.5	1.8 ± 0.4	104 ± 9	34	39	27	0.7
Mesoporous CoNi@Au	–1000	–2.5	1.7 ± 0.4	107 ± 12	29	31	40	0.1

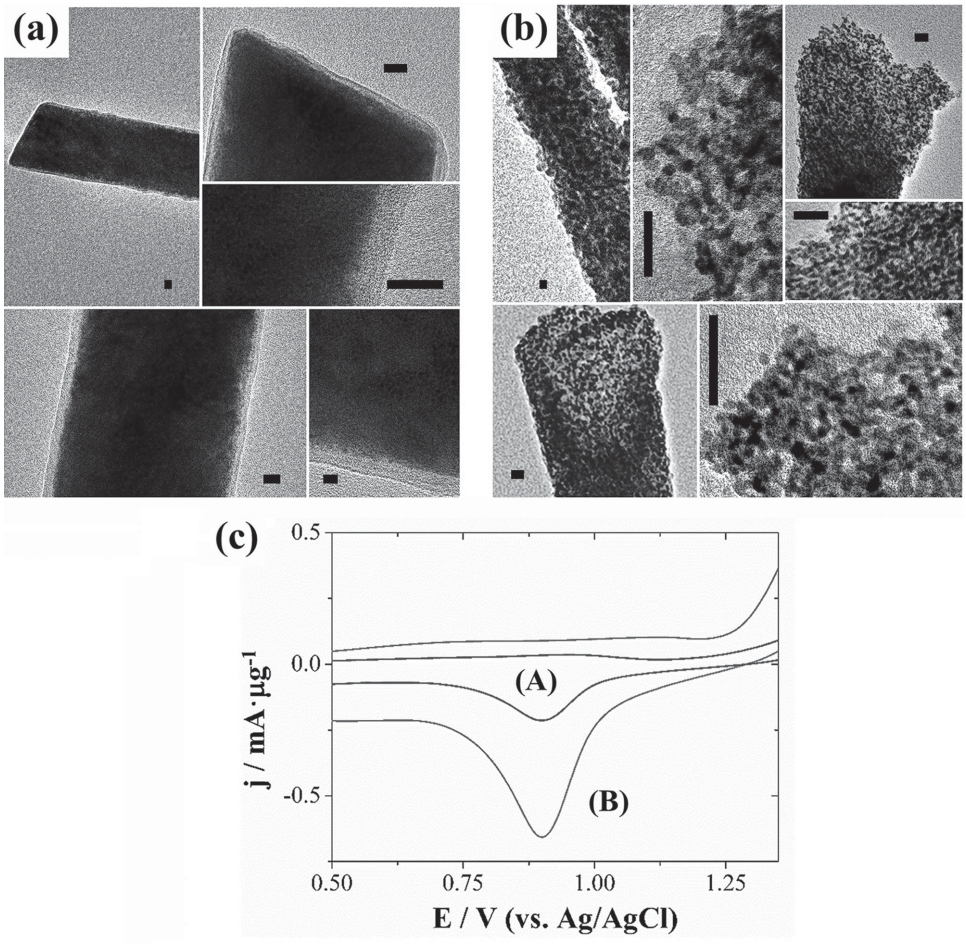

Figure 2. Transmission electron micrographs of the a) magnetic compact and mesoporous b) CoNi@Au NRs. c) Cyclic voltammetry (first cycle) of compact (A) and mesoporous (B) CoNi@Au NRs in H_2SO_4 0.5 M solutions at room temperature at the scan rate of 100 mV s^{-1}. Scale bar: 10 nm.

X-ray diffractograms (Figure 4S, Supporting Information) of both compact and mesoporous CoNi@Au nanorods show several peaks assigned to gold, given its presence in the shell and its significant diffracting response. Several peaks corresponding to the CoNi core were observed at 41.6°, 47.5°, 76.1°, 92.5°, and 98.7° 2θ, which respectively correspond to the (100), (101), (110), (112), and (004) peaks of a Co hexagonal close-packed (hcp) crystalline phase, albeit slightly distorted due to the presence of Ni in the alloy. Other peaks of the Co hcp phase can be masked by gold's diffraction peaks. A low proportion of a CoNi face-centered cubic (fcc) phase was detected at a peak of 51.6° 2θ. This primarily hcp crystalline structure has previously been obtained for CoNi films and nanorods.[18] Moreover, the selected area electron diffraction patterns of the synthesized nanorods (Figure 4Sa,b, Supporting Information) can be also indexed as the (002), (101), (110), and (100) orientations of the distorted Co hexagonal close-packed structure.

To use the nanorods synthesized as drug carriers, it is important to know the area that can effectively host pharmaceutical compounds. After covering them with the gold shell and recording the voltammetric response of the CoNi@Au nanorods in sulfuric acid, we therefore calculated the electrochemical surface area (ECSA) of each nanorod type. The charge associated with the reduction of gold oxide (Figure 2c) was proportional to the highly active area of the gold surface.[19] We were also to confirm the complete formation of the Au shell over the entire area of both structures, since nanorods supported on a glassy carbon (GC) electrode were immersed in a H_2SO_4 0.5 M solutions for 5 min, after which a successive cyclic voltammetry was performed. CoNi nanorods were etched and dissolved when unprotected by the Au shell after 5 min immersion in acidic media, which we verified by cyclic voltammetry that showed the response of the bare GC electrode. When the gold layer completely covered the nanorod, CoNi@Au was netter protected, even in H_2SO_4.

In sum, for both compact and mesoporous nanorods, the typical profile of gold in sulfuric solution was obtained (Figure 2c), even despite a high number of scans (>20). The voltammetric technique therefore allowed us to determine the immersion time that assures a complete gold layer on the surface of the nanorods. The stability of the CoNi@Au nanorods in the aggressive medium supposes their stability in a less aggressive (i.e., cellular) medium. The electrochemical surface area for both compact and mesoporous nanorods was 19 and 186 m^2 g^{-1}, respectively, while their Au shell thickness (ST) was 0.7 and 0.1 nm, also respectively (Table 1). The Au shell

thickness can be calculated from the ECSA values as follows (Equation (1))

$$ST = \frac{V_{Au}}{S_{Au}} = \frac{\left(\frac{m_{NR} \cdot P_{Au}}{\rho_{Au}}\right)}{ECSA \cdot m_{NR}} = \frac{P_{Au}}{ECSA \cdot \rho_{Au}} \quad (1)$$

where V_{Au} is the volume of Au shell, S_{Au} is the surface of Au shell, m_{NR} is the mass of one nanorod, P_{Au} ($g_{Au}/g_{CoNi@Au}$) is the weight percentage of Au of one nanorod, ECSA ($m^2/g_{CoNi@Au}$) is the mass-normalized electrochemical surface area, and ρ_{Au} (g_{Au}/cm^3) is the density of gold.

2.2. Nanorods Functionalization and Drug Loading, Magnetic Properties, and Drug Release

2.2.1. Functionalization and Drug Loading

Following the Au shell formation, the CoNi@Au nanorods were functionalized with thiol-poly(ethyleneglycol) (HS-PEG) or HS-PEG + CPT-11. First, the CoNi@Au-SH-PEG nanorods were used to detect the functionalization, whereas nanorods containing HS-PEG + CPT-11 were used to study the retention and release of the drug. Second, the CoNi@Au-SH-PEG nanorods were used to examine nanorods toxicity using HeLa cells, whereas the CoNi@Au-SH-PEG nanorods loaded with CPT-11 were used to investigate drug cytotoxicity delivered to HeLa cells via nanorod carriers. Finally, CoNi@Au-SH-PEG nanorods, both with and without CPT-11, were also used to gauge HeLa cells' uptake of nanorods by way of confocal microscopy.

Functionalization was performed by immersing the nanorods in a solution of the nonpolar organic thiol with or without the selected drug in stirring conditions (800 rpm) for 48 h, chiefly to form a highly stable organic monolayer due to the strong gold-sulfur bonding. **Figure 3**a portrays the overall strategy of the functionalization with HS-PEG + CPT-11 (i.e., drug-loading scheme). The HS-PEG monolayer rendered the nanorod surface hydrophilic and minimizes the aggregation of the magnetic nanorods favoring its interaction with cells, as well as incorporated and retained CPT-11 inside the polymeric network and inside the interconnected pore network in mesoporous structures. We hoped that the retention of the drug in the organic network would labile enough to make release moderately easy. Following the functionalization, the nonsedimentation of the nanorods was observed for 7 d, which signifies significant improvement in the stability of the suspension fundamental for biomedical applications. The procedure also afforded the modification of the surface properties of the nanorods – for example, in terms of surface charge and specific recognition of nanorods.

The formation and integrity of organic adsorbed layers onto the gold electrode was tested using voltammetric experiments,[13a] in which a close-packed layer of HS-PEG on the nanorod surface should hinder, if not block, the electrochemical superficial oxidation of the gold or the reduction of gold oxide, as well as the oxidation or reduction of species in solution on the nanorod surface. Therefore, to verify nanorod functionalization with HS-PEG, we performed electrochemical probe experiments by recording cyclic voltammetries of the Fe (II)/Fe (III) system in both CoNi@Au and CoNi@Au-SH-PEG NRs (Figure 3b). To that end, a drop of nanorod suspension was placed on the surface of a GC substrate and dried to obtain each GC-nanorod electrode. Figure 3b shows the typical reversible couple of the Fe (II)/Fe (III) system for the nonfunctionalized CoNi@Au nanorods. For the same amount of nanorods on

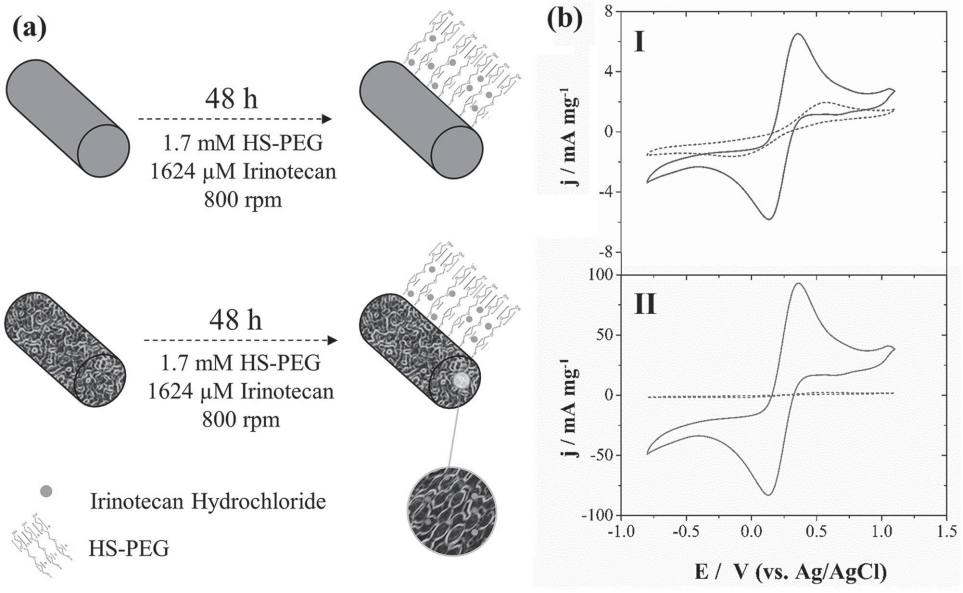

Figure 3. a) Schematic representation of nanorod functionalization with HS-PEG and drug loading. b) Cyclic voltammetries of the Fe (II)/Fe (III) system in a KNO_3 0.2 M + $K_4[Fe(CN)_6]$ 2×10^{-3} M + $K_3[Fe(CN)_6]$ 2×10^{-3} M solution on compact (b-I) and mesoporous (b-II) CoNi@Au (continuous lines) and in CoNi@Au-SH-PEG nanorods (dashed lines) placed on glassy carbon electrodes, at room temperature and at scan rate of 100 mV s^{-1}.

the GC surface, the detected current was significantly greater for mesoporous nanorods, which corresponds to the far greater effective area. The presence of the PEG layer in the CoNi@Au-SH-PEG nanorods caused a blocking effect of the surface of both mesoporous and compact CoNi@Au nanorods, thereby prompting a drastic decrease of the detected current. The electrochemical probe then allowed us to detect the functionalization of the nanorods with a HS-PEG layer. The faradaic Fe (II)/Fe (III) processes were strained with HS-PEG on the nanorods, though the electrochemical processes were not entirely hindered, which reveals that some mass transport of the Fe (II)/Fe (III) redox species occurs in the presence of the HS-PEG layer to the nanorods surface. This finding is important because the mass transport of the drug to the entire bulk should also be possible for drug release.

2.2.2. Magnetic Properties of the Functionalized Nanorods

The magnetic properties of the CoNi@Au nanorods, both compact and mesoporous, were analyzed before and after their functionalization with HS-PEG molecules. Figure 4Sc (Supporting Information) shows the normalized M/M_s (M: magnetization) curves for the four types of nanorod. The response of the functionalized nanorods was highly similar to that of the nonfunctionalized ones, which indicates that the presence of HS-PEG molecules does not preclude the manipulation of the magnetic nanorods. Indeed, they can be easily retained or targeted by applying a magnetic field. Compact CoNi@Au nanorods presented a soft-magnetic behavior, with a M_r/M_s = 0.3 (M_r: remanence) and a coercivity H_c = 230 Oe. Mesoporous CoNi@Au nanorods tended to exhibit superparamagnetic behavior, with low values for both remanence (M_r/M_s = 0.1) and coercivity (H_c = 50 Oe), a fact that favors their rapid response under an applied magnetic field and decreases their tendency to aggregate. In fact, both functionalized and nonfunctionalized mesoporous nanorods were easily maintained in suspension due to their magnetic properties and the low mass-per-volume of the unit.

When a suspension of nanorods was subjected to the action of a rotating magnetic field, the nanorods readily commenced a circular motion, with a rotational speed according to the applied magnetic field. Therefore, the magnetic character of the synthesized nanorods allowed handling during washing, targeting and accumulation in a defined target site, and movement in suspension.

2.2.3. Drug Release

The in vitro drug retention and release were studied via spectrofluorimetric assay after incubating both the compact and mesoporous nanorods with HS-PEG (CoNi@Au-SH-PEG) and CPT-11. The comparison of the fluorescence of the CPT-11 in a 10×10^{-3} M lactate buffered (pH 4.4) solution before and after its incubation with the nanorods and the HS-PEG (i.e., nanorod cofunctionalization) demonstrated drug retention in the lattice of the HS-PEG molecules, for compact nanorods, and also in the interior of the pores, for mesoporous nanorods. The maximum yield of CPT-11 retention in mesoporous nanorods was of 76%, a significantly higher value than the 36% retention efficiency of the compact CoNi@Au-SH-PEG nanorods. Mesoporous nanorods exhibited an increased ability to accumulate the drug and thus higher retention efficiency. That result could be the expected, given their exceptionally high pore volume, which can accommodate the drug.

The magnetic properties of the synthesized and functionalized nanorods were studied regarding the CPT-11 release in static conditions, as well as under the influence of an external rotatory magnetic field (20 Hz). The aim of these assays was to assess whether the drug release was magnetic-dependent and, thus, if the rate of release would be controllable. **Figure 4**a shows a diagram of the different release conditions considered in our work. Figure 4b–e shows the release profiles of CPT-11 trapped in CoNi@Au-SH-PEG nanorods. Irinotecan-loaded nanorods were first washed three times with 1 mL of the lactate-buffered medium and placed in 1 mL of the same buffer, after which the release of the drug was measured for 25 h. As Figure 4 shows, the release profiles of CPT-11 from compact and mesoporous nanorods, expressed as the percentage of the drug released, in static conditions and under the action of an external rotatory magnetic field, were highly similar. However, in absolute terms, significantly more CPT-11 was released with mesoporous structures, as expected, due to its superior load capability. Therefore, by using the mesoporous nanorods, the amount of nanocarriers needed to deliver the same amount of drug can be significantly reduced. Moreover, the magnetic-dependent release of the drug allows the modulation and control of its release rate. As such, the increased efficiency of drug release coupled with the possibility of the remote manipulation of the nanorods, by applying direct magnetic fields, and their rotational manipulation, by applying rotating fields, underscores mesoporous and compact nanorods as promising nanocarrier for cancer therapy. Magnetic nanorods can be considered smart nanocarriers because they have been engineered to provide a vast array of properties, including the ability to respond to the externally applied stimuli.

2.2.4. Cytotoxic Activity of CPT-11 Loaded CoNi@Au-SH-PEG NRs

The effectiveness of CPT-11-loaded CoNi@Au-SH-PEG nanorods was assessed and compared with that of the carrier (i.e., CoNi@Au-SH-PEG nanorods) by using the HeLa cell line. The survival of the cells, incubated for 24 h with a fixed amount of CPT-11 (0.027 and 0.080 μmol of CPT-11 for 20 μg mL^{-1} of compact and mesoporous nanorods, respectively), was evaluated 24 h after CPT-11 was removed from the culture medium. HeLa cells were incubated in the same conditions with empty CoNi@Au-SH-PEG nanorods, largely to study the toxicity effect of the carrier. The toxicity studies carried out with both carriers (Figure 5Sa,b, Supporting Information) showed that HeLa cells viability was greater than 90%, after incubation with empty compact and mesoporous CoNi@Au-SH-PEG nanorods, up to a concentration of 300 and 350 μg nanorods mL^{-1}, respectively. From these results we chose a concentration of 20 μg nanorods mL^{-1} to study the toxicity of CPT-11 trapped in the nanorods.

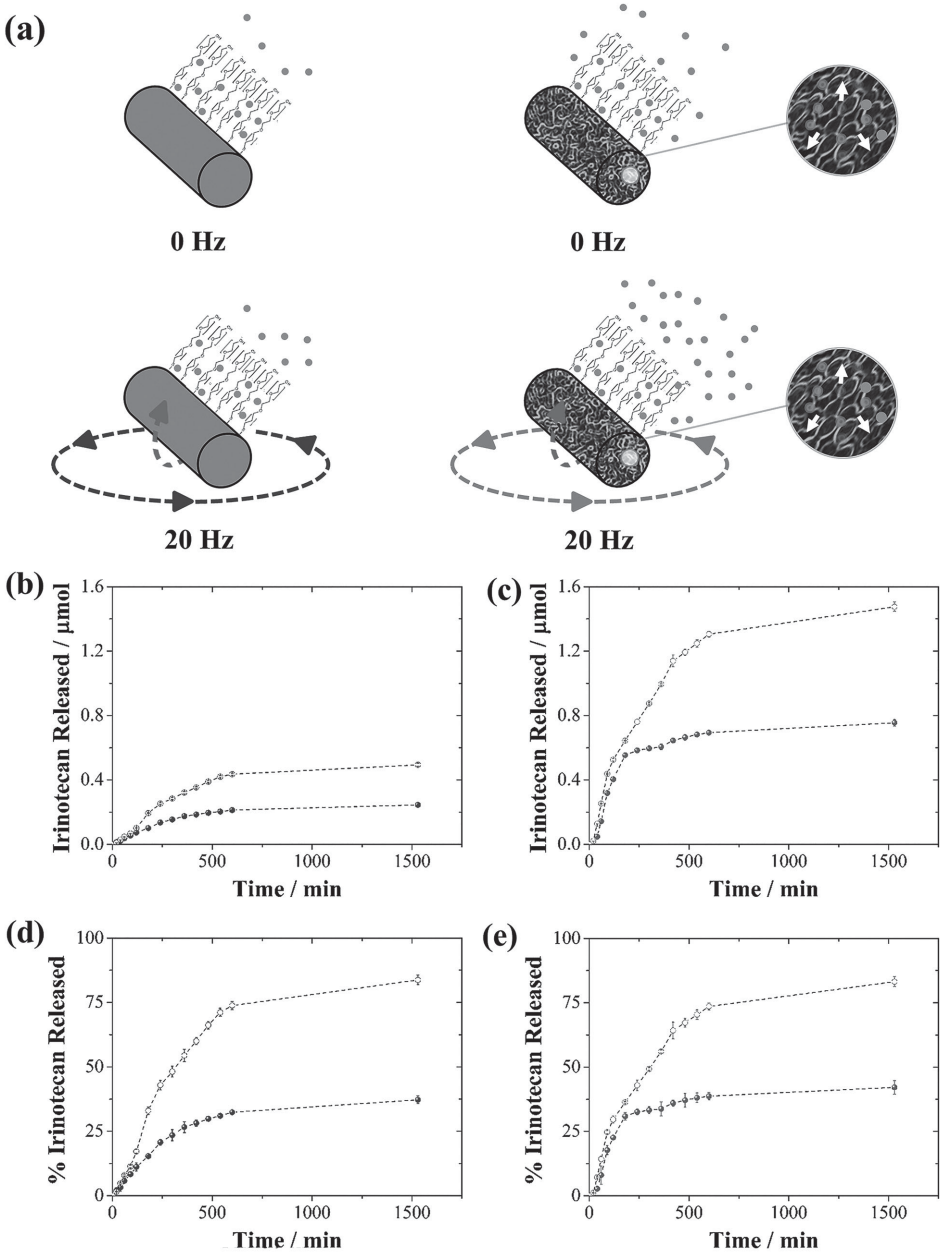

Figure 4. a) Schematic representation of CPT-11 release from magnetic compact (left) and mesoporous (right) CoNi@Au nanorods loaded with the drug in static conditions (upper) and under the influence of an external rotatory magnetic field of 20 Hz (bottom). b–e) Influence of the application of the external rotatory magnetic field on CPT-11 release from compact (b,d) and mesoporous (c,e) CoNi@Au nanorods (450 µg) expressed as the µmol of CPT-11 released (b,c) or as the percentage of the drug released (d,e) in static conditions (closed symbols) and under the influence of a magnetic external rotatory field (open symbols).

The cytotoxic effect of drug-loaded CoNi@Au-SH-PEG nanorods (**Figure 5**) was a function of the type of nanorod, either compact or mesoporous, and of the application, or not, of an external rotatory magnetic field. Cells were incubated 24 h with empty and CPT-11 loaded CoNi@Au-SH-PEG nanorods, and cell survival was evaluated by the tetrazolium dye (MTT) colorimetric assay 24 h after nanorod removal.

When using empty nanorods, cell survival was greater than 90% in silent (0 Hz) conditions, whereas the application of an external rotatory magnetic field (20 Hz) for 30 min caused a 44% and a 37% decrease in cell survival for compact and mesoporous nanorods, respectively. Cell death in the absence of CPT-11 when applied in an external rotating magnetic field could be attributed to a possible localized heating or a rotation of the nanorods inside the cells.

The incubation of HeLa cells with irinotecan-loaded compact and mesoporous CoNi@Au-SH-PEG nanorods in silent conditions (0 Hz) prompted 15.4% and 37.5% of cell death,

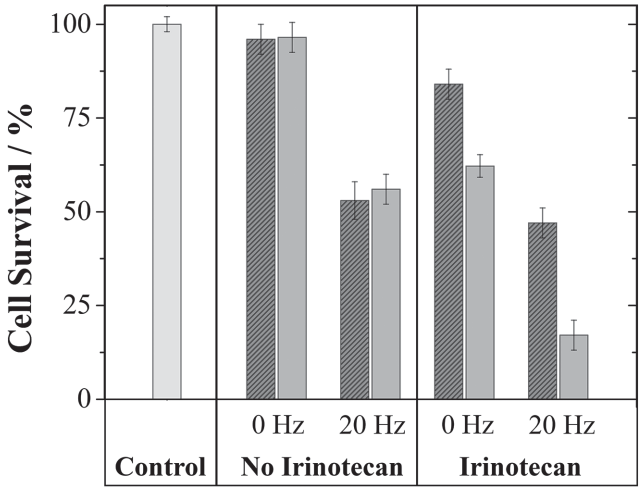

Figure 5. Surviving fraction of HeLa cells incubated with CPT-11 (left) for 48 h with cell culture medium, to which a 100% survival control was assigned; (middle) with 20 µg of empty compact (striped bars) or mesoporous (solid bars) CoNi@Au-SH-PEG nanorods mL^{-1} in silent (0 Hz) and under a rotatory external magnetic field (20 Hz); and (right) incubated with 20 µg of drug-loaded compact (striped bars) or mesoporous (solid bars) CoNi@Au-SH-PEG nanorods mL^{-1} in silent (0 Hz) and under a rotatory external magnetic field (20 Hz). CPT-11 content in incubates was 0.0013 or 0.0040 µmol $µg^{-1}$, respectively, with compact and mesoporous nanorods.

respectively. This result was consistent with the amount of CPT-11 released in the absence of magnetic field from a same amount of compact (0.01 µmol CPT-11 per 20 µg nanorods) or mesoporous (0.033 µmol CPT-11 per 20 µg nanorods) nanorods.

When the external rotatory magnetic field (20 Hz) was applied, after incubating the HeLa cells with the same amount of nanorods in the medium of that used in the absence of the magnetic field, a significant increase of cell death was observed in both cases. In those conditions, cell death was of 52.8% and 83.7% when HeLa cells were incubated with CPT-11 loaded in compact or mesoporous CoNi@Au-SH-PEG nanorods, respectively. Such increased cell death can be attributed to the sum of two factors: the largest release of CPT-11 when the magnetic field was applied (0.027 µmol CPT-11 per 20 µg compact nanorods and 0.080 µmol CPT-11 per 20 µg mesoporous nanorods) and the mechanical damage of cells due to the rotation of the nanorods inside the cells under the magnetic field effect.

When these results are compared with those obtained when CPT-11 was administered in a liposomal form, it has been shown that both liposomes and CoNi@Au-SH-PEG nanorods have excellent ability to incorporate the drug or to release it under specific stimuli: hyperthermia for thermosensitive liposomes or a magnetic field for CoNi@Au-SH-PEG nanorods.[3b] However, based on results from this study, mesoporous CoNi@Au-SH-PEG nanorods significantly improve the therapeutic effectiveness of irinotecan for anticancer therapy, compared to that of liposomes and other mesoporous structures, including lipid-coated mesoporous silica nanoparticles.[20] That benefit derives from magnetic actuation, which radically enhances killing efficiency and provides easy manipulation, magnetic targeting, and better control of the drug release rate. We can hypothesize that mesoporous CoNi@Au-SH-PEG nanorods therefore constitute an interesting alternative to other more usual nanocarriers to deliver different drugs.

2.2.5. Nanorods Uptake by HeLa Cells

CellTracker 5-chloromethylfluorescein diacetate (CMFDA) was used to demonstrate nanorod internalization by HeLa cells. CMFDA is a fluorescent chloromethyl derivative that freely diffuses through the membranes of live cells. Once inside the cells, these mildly thiol-reactive probes undergo what is thought to be a glutathion S-transferase-mediated reaction, in order to produce membrane-impermeable glutathion fluorescent dye adducts. A wide variety of applications were indicated for these dyes, including cell tracking in mixed cultures, long-term viability assays, and measuring cellular glutathione content using flow cytometry or the labeling of live cells.[21]

The green probe CMFDA stained the entire HeLa cells body, shown in green in **Figure 6**, which also shows nanorods, in red, that were visualized by reflection. The images show that HeLa cells internalize both compact and mesoporous CoNi@Au-SH-PEG nanorods, though that some nanorods remain extracellular.

The videos supplied (see Supporting Information) shows the 3D reconstruction of alive HeLa cells with compact

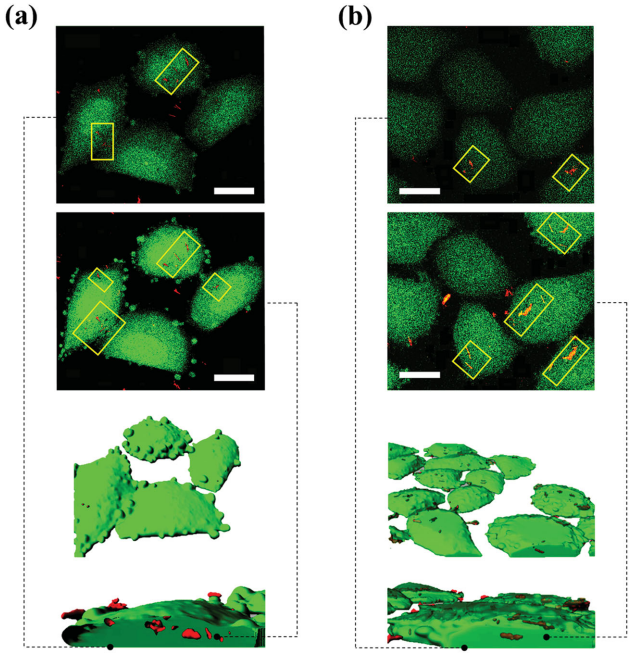

Figure 6. Internalization of compact (left) and mesoporous (right) CoNi@Au-SH-PEG nanorods by HeLa cells; HeLa cells cytoplasm stained with 5-chloromethylfluorescein diacetate is shown in green, and nanorods visualized by reflection are marked in red. Images are representative of two independent experiments: a 3D reconstruction of HeLa cells (bottom) and sections of HeLa cells acquired during scanning (top). Scale bar: 20 µm.

(Video 6S, Supporting Information) and mesoporous (Video 7S, Supporting Information) nanorods in their cytoplasm.

3. Conclusion

Electrochemical synthesis allowed us to prepare CoNi@Au-SH-PEG nanorods that demonstrated promise as magnetic nanocarriers for therapeutic molecules. Using aqueous solution allowed us to prepare compact, short (<2 µm) magnetic nanorods, whereas using ionic liquid-in-aqueous solution microemulsion allowed us to prepare mesoporous nanorods of similar dimensions and composition. The formation of a gold layer covering all of the nanorods, both compact and mesoporous, allowed their functionalization with a long HS-PEG molecule, which conferred hydrophilic character to the nanorods, favored their maintenance in suspension during several days by decreasing their aggregation, allowed them to retain the selected drug (i.e., CPT-11), and allowed their gradual release. The mesoporous CoNi@Au-SH-PEG nanorods present advantages with respect to the compact ones because they allow higher loading of drug in the interior of the pores, a higher loading of drug retained in more HS-PEG molecules adsorbed on the nanorods with higher area/volume, easy magnetic manipulation due to their specific magnetic properties, a lesser tendency toward sedimentation due to their lower mass, a lesser toxicity of carriers, and greater cell death efficiency with fewer carriers. The magnetic character of the mesoporous nanorods moreover favored magnetic manipulation, magnetic targeting, and accumulation, as well as the mechanical death of cellules accompanying the death produced by the drug.

4. Experimental Section

Electrochemical Media: The electrochemical media used to study the deposition process and to prepare nanorods were (i) an aqueous solution (W) of 0.2 M $CoCl_2{\cdot}6\ H_2O$ (Carlo Erba, >98.0%) + 0.9 M $NiCl_2$ (Panreac, >98%) + 30 g L^{-1} H_3BO_3 (Merck, 99.8%) + 0.7 g L^{-1} saccharin (Merck, >98%); (ii) an W + surfactant mixture (W + S) of 84.9 wt% of W + 15.1 wt% of p-octyl poly(ethylene glycol) phenyl ether also known as Triton X-100 (S) (Acros Organics, 98%); and (iii) ionic liquid-in-water (IL/W) microemulsions, prepared by mixing W, S, and 1-butyl-3-methylimidazolium hexafluorophosphate also known as $bmimPF_6$ ($C_8H_{15}F_6N_2P$, Solvionic, 99%) (IL) in proportions based on the literature (15.1 wt% of S, 1.1 wt% of IL, and 83.8% of W).[19] The mixture was sonicated for 5 min under argon bubbling, which prompted transparent stable microemulsions. Droplet size and the polydispersity index of microemulsions were analyzed by DLS with Zetasizer Nano ZS (Malvern Instruments).

Electrochemical Synthesis and Characterization: Electrochemical experiments were carried out using a microcomputer-controlled potentiostat/galvanostat Autolab with PGSTAT30 equipment and GPES software. As shown in the Supporting Information, the voltammetric study to find the optimum range of working potentials in aqueous (W), aqueous solution + surfactant (W + S), and ionic liquid-in-water (IL/W) microemulsions systems was performed at room temperature (25 °C), using a 3-electrode electrochemical system. Si/Ti (15 nm)/Au (100 nm) substrates (0.5 × 0.5 cm^2), Pt spiral, and Ag/AgCl/3 M KCl were used as working, counter, and reference electrodes, respectively. To define the nanorods structure polycarbonate membranes (20 µm thick, 100 nm nominal pore diameter, and 10^8– 2.5×10^9 pores cm^{-2} pore density with 100 nm thick gold layer in one side, which enabled conductivity) were used as working electrodes. After nanorod synthesis, the Au layer was removed by etching the Au using a saturated solution of I_2/I^-, and under ultrasonic stirring, the PC membranes were dissolved with chloroform (5×), and washed with chloroform (10×), ethanol (5×), and Millipore water (×5). Nanorods were also immersed in 0.1 M NaOH (3×) prior to being washed in Millipore water when microemulsions were employed. Finally, after the cleaning procedure, a thin, nanometric shell of gold formed via galvanic displacement, which consisted of immersing in 2.9×10^{-3} M of $HAuCl_4$ solution.

The morphology and structure of the CoNi@Au nanorods were examined by using transmission electron microscopy (Jeol 2100). Elemental composition was measured using electron probe microanalysis by energy-dispersive X-ray analysis (Cameca SX-50 equipment) or an X-ray analyzer incorporated in Leica Stereoscan S-360 equipment. XRD patterns were registered by means of a Philips MRD diffractometer with parallel optical geometry using a Cu Kα radiation ($\lambda = 1.5418$ Å). The electrochemical surface area of the different prepared nanorods was obtained by integrating the charge associated with the reduction of gold oxide, which was proportional to the real active surface area of the gold surface, in cyclic voltammograms recorded in H_2SO_4. Electrochemical surface area was estimated assuming that the charge required to reduce gold oxide was 390 µC cm^{-2}.[22]

Nanorod Functionalization and Drug Loading: Nanorods (900 µg) were functionalized by immersion in 2 mL of nonpolar organic thiol (1.7×10^{-3} M HS-PEG) with or without the selected drug (1.6×10^{-3} M irinotecan hydrochloride – Afine Chemicals,Hangzhou, China – which was pure, with a minimal grade of 99%.). Nanorod functionalization was corroborated by means of electrochemical probe experiments, namely by recording cyclic voltammetries of the Fe(II)/Fe(III) system in a KNO_3 0.2 M + 2×10^{-3} M $K_4[Fe(CN)_6]$ + 2×10^{-3} M $K_3[Fe(CN)_6]$ solution. For each experiment, suspensions of functionalized and nonfunctionalized nanorods were dropped onto the surface of a GC electrode (Metrohm) rod of 0.0314 cm^2 and dried under nitrogen flow. Drug retention analysis was performed by fluorescence emission and excitation spectra ($\lambda_{ex} = 278$ nm) using an AMINCO-Bowman Series 2 spectrofluorometer with a micro-cell (1 mL) at 25 °C. To determine the concentration of drug released, a calibration curve was necessary, which involved comparing the unknown concentration to a set of standard samples of known concentrations.

Cell Culture: Experiments were performed on the tumoral epithelial cell line HeLa originated from a cervix adenocarcinoma. HeLa cells were grown as monolayers in Dulbecco's modified Eagle's medium (DMEM) supplemented with 50 U mL^{-1} penicillin, 50 µg mL^{-1} streptomycin, 292 mg mL^{-1} L-glutamine, 1% nonessential amino acids, and fetal bovine serum at a final concentration of 10%; 4.5 g glucose L^{-1} (DMEM), fetal calf serum, penicillin-streptomycin, nonessential amino acids, and L-glutamine solutions were provided by from Biological Industries (Beit HaEmek, Israel). Cell cultures were performed in a humidified sterile atmosphere of 95% air and 5% CO_2 at 37 °C in a SteriCult 200 incubator (Hucoa-Erloss). HeLa cells were seeded in 25 cm^2 flasks (90 000 cells), in 35 mm Petri dishes (25 000 cells) or in an 8 well Nunc Lab-Tek II Chambered Coverglass (Thermo Scientific, USA) for confocal microscope studies. Cells were grown for 72 h and treated when cultures achieved exponential growth. All sterile plastics were from Corning (Corning, NY, USA).

Cells Treatment: The effect of nanorods with and without CPT-11 upon cell survival in silent conditions (0 Hz) and in the external rotatory magnetic field (20 Hz) was determined. HeLa cells seeded in 35 mm Petri dishes were cultured until reaching 70%–75% confluence and incubated for 24 h with functionalized nanorods (20 µg nanorods mL^{-1} DMEM), with and without CPT-11, in lactate buffer (10×10^{-3} M pH 4.4). The cells were next washed 3 times with sterile Dulbecco´s phosphate buffered saline (PBS), supplemented with fresh medium and incubated for another 24 h in silent conditions. To test the influence of an external rotatory magnetic field, the magnetic field (20 Hz) was applied for 30 min after washing with PBS. Cell survival was evaluated after 24 h of postincubation in a fresh medium by MTT (3-[4,5-dimethylthiazol-2-yl]-2,5-diphenyltetrazolium bromide) assay, which detected only living cells.[23]

That assay was based on the reduction of tetrazolium salt to form a formazan dye using the electrons from the mitochondria of viable cells. The appropriate amount of a MTT stock solution (1 mg mL^{-1} PBS) was added to DMEM for a final concentration of 47.6 μg mL^{-1}. The medium without MTT was withdrawn and replaced by the medium supplemented with the dye. Cells were incubated for 3 h at 37 °C, and to dissolve formazan precipitates, the medium was replaced by DMSO. Absorbance was measured at 526 nm on a Synergy H1 microplate spectrofluorimeter (SynergyMX, BioTek Instruments, Winooski, VT, USA). Cell survival was expressed as the percentage of absorption of treated cells in relation to that of control cells (100% survival).

Confocal Microscopy: Confocal microscopy was used to verify nanorods internalization. Cells were grown in an 8 well Nunc Lab-Tek II Chambered Coverglass. First, cells were incubated at 37 °C for 18 h with a suspension of the corresponding CoNi@Au-SH-PEG nanorods in DMEM (20 μg nanorods mL^{-1}) to allow their internalization. To confirm the intracellular localization of the nanorods, the cytoplasm of the cells was labeled with green CellTracker fluorescent probe CMFDA in serum-free culture medium, which acted as a cell tracker (C7025 Thermo Fisher, Life Technologies). The method of labeling consisted of five steps: (1) washing cells twice for 5 min with PBS, (2) incubating them for 30 min at 37 °C with the binding solution (5×10^{-6} M CMFDA in serum-free culture medium), (3) washing them twice for 5 min with PBS, (4) incubating them for 30 additional min at 37 °C with supplemented cell culture medium, and (5) ultimately washing them twice for 5 min with PBS. After labeling, the cells were maintained in complete culture medium containing 10×10^{-3} M HEPES to keep them alive during their observation with the microscope. HeLa cells were imaged using a Leica TCS SP2 confocal laser fluorescence microscope (Heidelberg, Germany) with simultaneous fluorescence and reflection acquisition, by using an argon laser of 488 nm. Different sections were initially scanned, and a data set of z-series images were collected from the bottom to top of the wells in the direction of the *z*-axis. 3D reconstructions were made with Imaris 7.2.3 (Bitplane AG, Zurich, Switzerland).

Supporting Information

Supporting Information is available from the Wiley Online Library or from the author.

Acknowledgements

This work was supported by the EU ERDF (FEDER) funds and the Spanish Government grant TEC2014-51940-C2-2-R from Ministerio de Economía y Competitividad (MINECO). A.S. thanks the Ministerio de Educación, Cultura y Deporte for a predoctoral grant (FPU). Authors thank the CCiT-UB for the use of their equipment. Authors are also grateful to Dr. Raimundo Gargallo (Department of Analytical Chemistry, University of Barcelona) for his support in the fluorimetry experiments and to Dr. Manel Bosch (Advanced Optical Microscopy Unit of the CCiT-UB) for his helpful technical support in the confocal experiments.

Received: March 22, 2016
Revised: May 24, 2016
Published online: July 18, 2016

[1] a) N. Nasongkla, E. Bey, J. Ren, A. Hua, C. Khemtong, J. S. Guthi, S.-F. Chin, A. D. Sherry, D. A. Boothman, J. Gao, *Nano Lett.* **2006**, *6*, 2427; b) P. Kesharwani, K. Jain, N. K. Jain, *Prog. Polym. Sci.* **2014**, *39*, 268; c) J. C. Kraft, J. P. Freeling, Z. Wang, R. J. Y. Ho, *J. Pharm. Sci.* **2014**, *103*, 29; d) D. M. Copolovic, K. Langel, E. Eriste, U. Langel, *ACS Nano* **2014**, *8*, 1972; e) J. Kreuter, *Adv. Drug Delivery Rev.* **2014**, *71*, 2; f) A. Wicki, D. Witzigmann, V. Balasubramanian, J. Huwyler, *J. Control. Rel.* **2015**, *200*, 138.

[2] a) A. V. Kabanov, E. V. Batrakova, V. Y. Alakhov, *J. Control. Rel.* **2002**, *82*, 189; b) L. C. Glangchai, M. Caldorera-Moore, L. Shi, K. Roy, *J. Control. Rel.* **2008**, *125*, 263; c) S. Panja, S. Maji, T. K. Maiti, S. A. Chattopadhyay, *ACS Appl. Mater. Interfaces.* **2015**, *7*, 24229.

[3] a) M. García-Díaz, M. Kawakubo, P. Mroz, M. L. Sagristá, M. Mora, S. Nonell, M. R. Hamblin, *J. Control. Rel.* **2012**, *162*, 355; b) A. Casadó, M. L. Sagristá, M. Mora, *J. Pharm. Sci.* **2014**, *103*, 3127.

[4] a) W. Park, B.-C. Bae, K. Na, *Biomaterials* **2016**, *77*, 227; b) Y. Shamay, L. Adar, G. Ashkenasy, A. David, *Biomaterials* **2011**, *32*, 1377; c) L. Momtazi, S. Bagherifam, G. Singh, A. Hofgaard, M. Hakkarainen, W. R. Glomm, N. Roos, G. M. Maelandsmo, G. Griffiths, B. Nyström, *Langmuir* **2014**, *433*, 76; d) F. Liu, V. Kozlovskaya, S. Medipelli, B. Xue, F. Ahmad, M. Saeed, D. Cropek, E. Kharlampieva, *Chem. Mater.* **2015**, *27*, 7945; e) Y. Wen, J. K. Oh, *Colloid Surf. B* **2015**, *133*, 246.

[5] a) L. A. Torre, F. Bray, R. L. Siegel, J. Ferlay, J. Lortet-Tieulent, A. Jernal, *CA-Cancer J. Clin.* **2015**, *65*, 87; b) J. Ferlay, I. Soerjomatarm, R. Dikshit, S. Eser, C. Mathers, M. Rebelo, D. M. Parkin, D. Forman, F. Bray, *Int. J. Cancer.* **2015**, *136*, 359; c) J. Ferlay, E. Steliarova-Foucher, J. Lortet-Tieulent, S. Rosso, J. W. W. Coebergh, H. Comber, D. Forman, F. Bray, *Eur. J. Cancer.* **2013**, *49*, 1374; d) M. Arnold, H. E. Karim-Kos, J. W. Coebergh, G. Byrnes, A. Antilla, J. Ferlay, A. G. Renehan, D. Forman, I. Soerjomatarm, *Eur. J. Cancer.* **2015**, *51*, 1164.

[6] a) K. Suda, K. Sato, H. Mizuuchi, Y. Kobayashi, M. Shimoji, K. Tomizawa, T. Takemoto, T. Iwasaki, M. Sakaguchi, T. Mitsudomi, *Resp. Investigation* **2014**, *52*, 322; b) S. Singhal, L. R. Kaiser, *Surg. Oncol. N. Am.* **1998**, *7*, 505; c) G. N. Marta, F. Y. De Moraes, *Exp. Rev. Anticancer Ther.* **2015**, *15*, 1257.

[7] a) J. Tabernero, E. V. Cutsem, R. Lakomy, J. Parausová, P. Ruff, G. A. Van Hazel, V. M. Moiseyenko, D. R. Ferry, J. J. McKendrick, K. Soussan-Lazardi, S. Chevalier, C. J. Allerga, *Eur. J. Cancer.* **2014**, *50*, 320; b) C. Fuchs, E. P. Mitchell, P. M. Hoff, *Cancer Treat. Rev.* **2006**, *32*, 491; c) M. Z. Ahmad, S. Akhter, M. Anwar, A. Kumar, M. Rahman, A. H. Talasaz, F. J. Ahmad, *Drug Dev. Ind. Pharm.* **2013**, *39*, 1936.

[8] a) M. J. O'Connell, *J. Clin. Oncol.* **2009**, *27*, 3082; b) V. P. Torchilin, *Nat. Rev. Drug Discovery* **2014**, *13*, 813; c) S. Mura, J. Nicolas, P. Couvreur, *Nat. Mater.* **2013**, *12*, 991; d) C. L. Weaver, J. M. LaRosa, X. Luo, X. T. Cui, *ACS Nano* **2014**, *8*, 1834; e) J. Di, S. Yao, Y. Ye, Z. Cui, J. Yu, T. K. Ghosh, Y. Zhu, Z. Gu, *ACS Nano* **2015**, *9*, 9407.

[9] M. García-Díaz, S. Nonell, A. Villanueva, J. C. Stockert, M. Cañete, A. Casadó, M. Mora, M. L. Sagristá, *Biochim. Biophys. Acta* **2011**, *1808*, 1063.

[10] a) K. M. Pondman, N. D. Bunt, A. W. Maijenburg, R. J. A. Van Wezel, U. Kishore, L. Abelman, J. E. Ten Elshof, B. Ten Haken, *J. Mag. Mag. Mater.* **2015**, *380*, 299; b) K. M. Pondman, A. W. Maijenburg, F. B. Celikkol, A. A. Pathan, U. Kishore, B. Ten Haken, J. E. Ten Elshof, *J. Mater. Chem.* **2013**, *1*, 6129; c) S. N. Tabatabaei, H. Girouard, A.-S. Carret, S. Martel, *J. Control Rel.* **2015**, *206*, 49; d) J. Wang, C. Gong, Y. Wang, G. Wu, *Colloid Surface. B* **2014**, *118*, 218.

[11] a) K. Tschulik, K. Ngamchuea, C. Ziegler, M. G. Beier, C. Damm, A. Eychmueller, R. C. Compton, *Adv. Funct. Mater.* **2015**, *25*, 5149; b) M. F. Contreras, R. Sougrat, A. Zaher, T. Ravasi, J. Kosel, *J. Nanomedicine* **2015**, *10*, 2141; c) K. Giannousi, M. Menelaou, J. Arvanitidis, M. Angelakeris, A. Pantazaki, C. Dendrinou-Samara, *J. Mater. Chem. B* **2015**, *3*, 5341.

[12] a) D.-H. Kim, E. A. Rozhkova, I. V. Ulasov, S. D. Bader, T. Rajh, M. S. Lesniak, V. Novosad, *Nat. Mater.* **2010**, *9*, 165; b) T. Vemulkar, R. Mansell, D. C. M. C. Petit, R. P. Cowburn, M. S. Lesniak, *Appl.*

Phys. Lett. **2015**, *107*, 012403; c) P. Tiberto, G. Barrera, F. Celegato, G. Conta, M. Coïsson, F. Vinai, F. Albertini, *J. Appl. Phys.* **2015**, *117*, 17B304.

[13] a) C. Gispert, A. Serrà, M. A. Alea, M. Rodrigues, E. Gómez, M. Mora, M. L. Sagristá, L. Pérez-Garcia, E. Vallés, *Electrochem. Commun.* **2016**, *63*, 18; b) N. Choi, Y. Guan, L. Yang, L. Jia, X. Wei, H. Liu, C. Guo, *J. Colloid Interface Sci.* **2013**, *395*, 50.

[14] a) K. Keshoju, H. Xing, L. Sun, *Appl. Phys. Lett.* **2007**, *91*, 123114; b) A. Güntherm, P. Bender, A. Tschöpe, R. Birringer, *J. Phys. Condens. Matter.* **2011**, *23*, 325103.

[15] a) R. Ferré, K. Ounadjela, J. M. George, L. Piraux, S. Dubois, *Phys. Rev. B* **1997**, *56*, 66; b) Y. Zhao, H. Zeng, *IEEE Trans Nanobioscience* **2009**, *8*, 226; c) N. Gao, H. Wang, E. H. Yang, *Nanotechnology* **2010**, *21*, 105107; d) D. Choi, A. Fung, H. Moon, D. Ho, Y. Chen, E. Kan, Y. Rheem, B. Yoo, N. Myung, *Biomed. Microdevices* **2007**, *9*, 143; e) A. Hultgren, M. Tanase, C. S. Chen, G. J. Meyer, D. H. Reich, *J. Appl. Phys.* **2003**, *93*, 7554; f) A. Hultgren, M. Tanase, E. J. Felton, K. Bhadriraju, A. K. Salem, C. S. Chen, D. H. Reich, *Biotechnol. Prog.* **2005**, *21*, 509.

[16] a) Y. Rheem, B.-Y. Yoo, W. P. Beyermann, N. V. Myung, *Nanotechnology* **2007**, *18*, 125204; b) J. Vilana, E. Gómez, E. Vallés, *J. Electroanal. Chem.* **2013**, *703*, 88.

[17] a) A. Serrà, E. Gómez, E. Vallés, *Electrochim. Acta.* **2015**, *174*, 630; b) A. Serrà, E. Gómez, E. Vallés, *Int. J. Hydrog. Energy* **2015**, *40*, 8062; c) A. Serrà, E. Gómez, I. V. Golosovsky, J. Nogués, E. Vallés, *J. Mater. Chem. A* **2016**, *4*, 7805.

[18] a) J. Vilana, R. Amade, S. Hussain, E. Bertran, E. Gómez, E. Vallés, *Mater. Lett.* **2014**, *124*, 8; b) G. Ali, M. Maqbool, *Nanoscale Res. Lett.* **2013**, *8*, 352.

[19] a) A. Serrà, E. Gómez, J. F. López-Barbera, J. Nogués, E. Vallés, *ACS Nano* **2014**, *8*, 4630; b) Y. Gao, S. Han, B. Han, G. Li, D. Shen, Z. Li, J. Du, W. Hou, G. Zhang, *Langmuir* **2005**, *21*, 568.

[20] a) X. Liu, A. Situ, Y. Kang, K. R. Villabroza, Y. Liao, C. H. Chang, T. Donahue, A. E. Nel, H. Meng, *ACS Nano* **2016**, *10*, 2702; b) S. Nastase, L. Bajenaru, D. Berger, C. Matei, M. G. Moisescu, D. Constantin, T. Savopol, *Cent. Eur. J. Chem.* **2014**, *12*, 813.

[21] a) R. P. Haugland, *Handbook of Fluorescent Probes and Research Chemicals*, 7th ed, Eugene, Oregon **1999**; b) G. Packroff, J. R. Lawrence, T. R. Neu, *Acta Protozool.* **2002**, *41*, 245; c) K. S. Ralston, M. D. Solga, N. M. Mackey-Lawrence, A. Somlata, A. Bhattacharya, W. A. Petri Jr., *Nature* **2014**, *508*, 526.

[22] a) S. Trasatti, O. A. Petrii, *Pure Appl. Chem.* **1991**, *63*, 711; b) F. Jia, C. Yu, Z. Ai, L. Zhang, *Chem. Mater.* **2007**, *19*, 3648.

[23] T. Mosmann, *J. Immunol. Methods* **1983**, *65*, 55.